Cryo-EM structures of adenosine receptor A_3AR bound to selective agonists

Hongmin Cai[1,7,*], Shimeng Guo[1,7], Youwei Xu[1,7], Zhikan Xia[1,7], Junrui Li[1], Jun Sun[1,2], Yi Jiang[3], Xin Xie[1,2,4,5,6,*], H. Eric Xu[1,2,5,*]

[1] State Key Laboratory of Drug Research, Shanghai Institute of Materia Medica, Chinese Academy of Sciences, Shanghai, China.

[2] University of Chinese Academy of Sciences, Beijing, China.

[3] Lingang Laboratory, Shanghai, China.

[4] School of Pharmaceutical Science and Technology, Hangzhou Institute for Advanced Study, University of Chinese Academy of Sciences, Hangzhou, China.

[5] School of Life Science and Technology, ShanghaiTech University, Shanghai, China.

[6] Shandong Laboratory of Yantai Drug Discovery, Bohai Rim Advanced Research Institute for Drug Discovery, Yantai, China

[7] These authors contributed equally: Hongmin Cai, Shimeng Guo, Youwei Xu, Zhikan Xia

***Correspondence:** caihongmin@simm.ac.cn (H.C.); xxie@simm.ac.cn (X.X.); eric.xu@simm.ac.cn (H.E.X.)

Abstract

The adenosine A3 receptor (A_3AR) belongs to a subfamily of G protein-coupled receptors and is an important therapeutic target for conditions including inflammation and cancer. The clinical compounds CF101 and CF102 are potent and selective A_3AR agonists, but the structural basis of their recognition was unknown. Here we present the cryogenic electron microscopy structures of the full-length human A_3AR bound to CF101 and CF102 at 3.3-3.2 Å resolution in complex with heterotrimeric G_i protein. These agonists bind within the orthosteric pocket, with their adenine components engaging in conserved interactions while their substituted 3-iodobenzyl groups exhibit different orientations. Swapping extracellular loop 3 (ECL3) of A_3AR onto other adenosine receptor subtypes enabled CF101/CF102 binding and receptor activaton, and mutations in key residues, including $His^{3.37}$, $Ser^{5.42}$ and $Ser^{6.52}$ that form a unique subpocket in A_3AR, abolished receptor activation, highlighting these structural elements are critical for ligand selectivity. Compared to inactive A_{2A}AR, the A_3AR structures reveal conserved mechanism of receptor activation, including an outward shift of TM6. These structures provide key insights into molecular recognition and signaling mechanisms of A_3AR, which should aid rational design of subtype-selective ligands targeting this important class of adenosine receptors.

Introduction

The adenosine receptor subfamily of G protein-coupled receptors consists of four subtypes: A_1, A_{2A}, A_{2B}, and A_3[1, 2]. These receptors are activated by the endogenous ligand, adenosine, to transduce downstream signals that mediate a number of important physiological and pathalogical roles including immunomodulation, energy balance, cardiac function, neuroprotection, etc [3-5]. A_3AR is expressed in various tissues including the brain, heart, lungs, liver, kidneys, and immune cells[6]. Through its signaling functions, A_3AR participates in regulating cardiac function, vasodilation, inhibition of inflammation, protection against ischemia-reperfusion injury, and suppression of oxidative stress. Additionally, A_3AR is highly expressed in a number of tumor cells, suggesting its potential as a therapeutic target for suppressing cancer cell proliferation[6-8].

The activation of A_{2A}AR and A_{2B}AR predominantly elicits stimulatory G protein (G_s) signaling, while A_1AR and A_3AR exhibit a preference for coupling to inhibitory G protein (G_i), leading to inhibition of adenylate cyclase and decreased intracellular cyclic AMP[2]. Based on the chemical structure of adenosine, numerous agonists and antagonists have been designed and tested against A_3AR for disease indications such as cancer, inflammation, and pain[9] . Previous studies suggest that modifications at the N^6 position on the purine and 5'-N position on ribose group based on the adenosine framework yield potent A_3AR agonists with high subtype selectivity[10-12]. CF101 and CF102 are representatives of such modification strategy with similar nucleoside core structure and only one chloro-substituent difference, both demonstrate high affinity and selectivity for A_3AR[13-15]. CF101 showed efficacy in Phase III trials for psoriasis and rheumatoid arthritis[6] while CF102 is in clinical trials for hepatocellular carcinoma and non-alcoholic steatohepatitis (NASH)[16, 17].

Adenosine receptors mediate many important functions and their wide expression makes subtype selectivity of ligands more critical to reduce possible side effects [18, 19]. Elucidating the structural basis of selective ligand binding to A_3AR could help in improving the drug design process. To date, no A_3AR structure has been reported. In this paper, we present the cryo-EM structures of A_3AR bound to G_i in the presence of CF101 and CF102, which reveals the basis of ligand recognition and ligand-induced activation mechanism of A_3AR. Our works provide important insights for designing effective A_3AR-targeted therapies, and more broadly for the subfamily of adenosine receptors.

Results and Discussion

Overall structures of the complexes

CF101 and CF102 are A_3AR agonists containing modifications to the ribose and adenine moieties that confer potent binding to A_3AR (Fig. 1a). Specifically, CF101 and CF102 have a

5'-N-methylcarboxamide substitution on the ribose group and a N^6-(3-iodobenzyl) substitution on the adenine base (Fig. 1a). These modifications result in significantly higher A_3AR potency compared to the endogenous A_3AR agonist adenosine. We verified the selectivity of these nucleoside-derived compounds for A_3AR versus other adenosine receptor subtypes (A_1/A_{2A}/A_{2B}-AR) using NanoBiT association assays (Fig. 1b-d). While adenosine activated four subtypes with similar micromolar potencies, CF101 and CF102 displayed strongest potency of ~3 nM on A_3AR but had weak or negligible response on other subtypes of adenosine receptors.

We used NanoBiT tether strategy to stabilize the full-length A_3AR-G protein complexes, as it has been used for many GPCR structural studies[20-22] (Supplementary Fig. 1). A_3AR used in this study had an N-terminal thermostabilized apocytochrome b562RIL (BRIL) fusion to enhance its expression, which is co-expressed with G protein subunits and scFv16, an antibody fragment that is used to further stabilize the receptor G protein complex. For the CF101-A_3AR-G_i complex, data from 20,779 movies comprising 271,323 particles was used to determined the structure at 3.29 Å resolution (Supplementary Fig. 2, Supplementary Table 1). For the CF102-A_3AR-G_i complex, data from 13,581 movies yielding 283,561 particles was used to determined the structure at a resolution of 3.19 Å (Supplementary Fig. 3, Supplementary Table 1). The structures of the CF101/CF102-A_3AR-G_i complexes revealed that the ligands occupy the orthosteric binding pocket, with the core structures modeled clearly into the cryo-EM density at the center of the receptor transmembrane helicals (TMs) (Fig. 1e-h).

The structures showed the canonical seven-transmembrane architecture for A_3AR, with the intracellular domains occupied by the α5 helix of $G\alpha_i$ for G_i coupling. The density maps enabled modelling of most of the structures, except for A_3AR N-terminus residues M1-L8, third intracellular loop N211-Y222, C-terminus V301-E318, and the alpha-helical domain of $G\alpha_i$. The extracellular loop M151-S165 was also less defined but the backbone could be established (Supplementary Fig. 4). Aside from these regions, the models were well-resolved. Overall, the two agonist-bound complexes were highly similar, with 0.593 Å root mean square deviation (RMSD) for the whole receptor.

Binding mode of CF101/CF102 in A_3AR orthosteric site

The A_3AR agonists CF101 and CF102 bind at conserved orthosteric pocket formed by ECL2, TM3, TM5, TM6 and TM7, akin to the endogenous ligand adenosine bound to other adenosine receptor subtypes (Fig. 2a-b). However, the orientations of the modified 3-iodobenzyl moieties differ between CF101 and CF102. The adenine core mediates conserved receptor interactions commonly seen in other adenosine receptors[21, 23, 24]. Notably, the adenine pyrimidine forms

π-stacks against $F^{45.52}$, and the $F^{45.52}$A mutation greatly affected the ability of CF101/CF102 to induce the receptor activation (Fig. 2c-f, Supplementary Table 2). Additionally, ribose and 3-iodophenyl groups form hydrogen bonds with polar side chains at positions 3.36, 6.55 and 7.43, which are key for recognition of nucleoside ligands by all adenosine receptors (Fig. 2c-f, Supplementary Table 2).

The ligand binding pocket is mainly comprosed of hydrophobic residues, including position 3.33, 5.38, 5.47, 6.48, 6.51 and 7.39, which form hydrophobic contacts that are important for CF101/CF102 potencies (Fig. 2c-f, Supplementary Table 2). Alanine mutations at these positions severely reduced agonists' ability to induce receptor activation. $His^{3.37}$ and $Ser^{5.42}$ participate van der Waals contacts with the bound ligands, their alanine mutations also affected activity (Fig. 2c-f, Supplementary Table 2). The side chains from $M174^{5.35}$ and $L264^{7.35}$ in the receptor form hydrophobic interactions with the 3-iodophenyl group extended from the N^6 position of the adenosine base of CF101. In contrast, the corresponding group of CF102 is surrounded by $V169^{ECL2}$ and $L264^{7.35}$ from the receptor. Alanine mutations on these residues did not significantly affect the potency of the compounds on A_3AR (Supplementary Fig. 6a, Supplementary Table 2), suggesting that the 3-iodophenyl substituents may exist alternative states at the receptor extracellular domains. This demonstrates that the N^6 position may accommodate various substituted groups through distinct conformations in the A_3AR pocket.

Moreover, CF102 is a 2-chloro derivative of CF101 (Fig. 1a). $Y15^{1.35}$ in CF102-bound A_3AR forms hydrophobic contact with the 2-chloro group in CF102. Meanwhile, $Y15^{1.35}$ in A_3AR formed π-π interaction with $Y265^{7.36}$ in TM7. The $Y15^{1.35}$A mutation in A_3AR abolishes the agonist activity of both CF102 and CF101 (Fig. 2c-f, Supplementary Table 2). According to the reports, modifications to the 2-position of the adenosine structure tend to well-tolerated in binding A_3AR[14], whether it a small or large group, even the macrocycle group linked with the group from N^6 moeity[25]. Elucidation of the subtle structural variations in ligand and receptor interactions thus provides molecular insight into the conformational adaptability and binding pose governing molecular recognition at A_3AR.

ECL3 in adenosine receptors

CF101 and CF102 show high selectivity on A_3AR rather than other subtypes. Analysis the sequence of adenosine receptors reveals strong conservation within TMs, while the extracellular loops diverge among subtypes (Supplementary Fig. 5). ECL1 shows relatively distant from the orthosteric site. $F168^{45.52}$ in ECL2 provides the key π-π interactions with each agonists in adenosine receptors. However, A_3AR possesses a shorter ECL3 than other subtypes (Fig. 3a). The shorter ECL3 may rigidify A_3AR to minimize its conformational changes for specific ligand binding.

To assess the role of ECL3 in A_3AR, we engineered chimeric receptors by grafting ECL3 from A_3AR onto the backbones of other adenosine receptors. The chimeric receptors gained the ability to bind CF101 and CF102 with increased efficacy or potency (Fig. 3b-c, Supplementary Table 3). These findings suggest that ECL3 could serve as a structural factor mediating the selective recognition CF101 and CF102 by A_3AR. According to the reported structure-activity relationship of ligands at the A_3AR, numerous N^6-substituted adenosine derivatives were synthesized. Too small or bulky groups at the N^6 position would reduce its potency or affinity on A_3AR[13, 14]. The N^6 position on adenosine is projecting outwards into the binding pocket of A_3AR and is in close spatial proximity to the ECL3 region of the A_3AR. So the ECL3 loop is an important consideration in structure-activity studies of N^6-modified adenosine derivatives against adenosine receptors. Delineating these subtle structural variations provides molecular insight into the selectivity of structurally analogous ligands for adenosine receptors.

Binding pocket residues across adenosine receptors

Furthermore, A_3AR shared lowest identity with other subtypes among adenosine receptors. The sequence analysis reveals that the A_3AR may confer selectivity through different residue types in the orthosteric binding pocket (Fig. 4a), which include residues at positions 3.32 (L/V/V/V, the residue in A_3/A_1/A_{2A}/A_{2B}-AR), 3.37 (H/Q/Q/Q), 5.42 (S/N/N/N), 5.47 (I/V/V/V), 6.52 (S/H/H/H) and 6.58 (I/T/T/T) (Fig. 4b, Supplementary Fig. 7). These residues in A_3AR were mutated to the corresponding residues of other receptor subtypes, with aim to assess the impact of these A_3AR mutants on the activity of CF101 and CF102 (Fig. 4c-d).

The leucine at position 3.32 in A_3AR, versus valine in other subtypes, did not affect CF101/CF102 activity when mutated to valine, consistent with similar hydrophobic properties (Fig. 4c-d, Supplementary Fig. 7, Supplementary Table 2). Likewise, mutating isoleucine at positions 5.47 and 6.58 in A_3AR to the valine and threonine found in other subtypes slightly impacted activation (Fig. 4c-d, Supplementary Table 2). This suggests that the slightly shorter side chains present in valine and threonine do not impair binding.

The side chain of $H^{3.37}$ and $S^{5.42}$ in A_3AR form a hydrogen bond , which could not be formed by corresponding residues $Q^{3.37}$ and $N^{5.42}$ in other adenosine receptor subtypes (Fig. 4e-i). The $H^{3.37}Q$ mutation showed a limited impact on the activity of CF101/CF102 but the $S^{5.42}N$ mutation almost abolished the ability of CF101/CF102 to induce the receptor activation (Fig. 4c-d, Supplementary Table 2). Additionally, mutating $S^{6.52}$ to histidine (H) also severely decreased CF101 and CF102 activity, likely due to unfavorable steric or electronic properties of the longer histidine side chain (Fig. 4c-d, Supplementary Fig. 7, Supplementary Table 2). In contrast to other adenosine receptor subtypes, $H^{3.37}$, $S^{5.42}$ and $S^{6.52}$ form a distinctive

subpocket in A_3AR to accommodate the 5'-N-methylcarboxamide from the ribose (Fig. 4e-i, Supplementary Fig. 8). These results implicate this microdomain serves as a structural determinant for stabilizing CF101 and CF102 in A_3AR versus other subtypes. Together, these findings demonstrate that minor sequence changes in the receptors could impact their conformations, thereby affecting ligand binding specificity.

The activation mechanism of adenosine receptor A_3AR

Structural comparisons between active, agonist-bound A_3AR complexes and an inactive, antagonist-bound A_{2A}AR structure (PDB ID: 4EIY)[26] reveal hallmarks of conformational changes associated with GPCR activation[27, 28]. The A_3AR structures exhibit an outward movement of TM6 compared to inactive A_{2A}AR, shifting 11.6 Å based on measurements of residue $Glu^{6.30}$ at Cα atoms in receptors, analogous to movements seen in other activated class A GPCRs upon G protein coupling (Fig. 5a). Additional rearrangements of activation include inward movements of TM1 and TM7 and an upward shift of TM3 in A_3AR relative to inactive A_{2A}AR (Fig. 5b-d). The A_3AR agonists CF101 and CF102 dock deeper into the orthosteric pocket compared to the A_{2A}AR antagonist ZM-241385, enabling engagement of conserved GPCR activation motifs like the “toggle switch” on $W^{6.48}$ and transmission switch motifs $D^{3.49}R^{3.50}Y^{3.51}$ and $N^{7.49}P^{7.50}xxY^{7.53}$ (Fig. 5e-h). These microswitches trigger the conformational changes from the ligand binding pocket to the cytoplasmic G protein coupling interface. The series of structural transitions led to the rearrangements of receptor to enable G protein coupling and activation. By providing near-atomic resolution of A_3AR activation mechanisms, these findings reveal fundamental insights into the relationship between ligand recognition in receptor, and activation of downstream signaling.

G protein coupling of adenosine receptors

All adenosine receptors exhibit differential G protein coupling preferences that correlate with distinct conformational orientations of the associated G proteins[21, 23, 24]. A_1AR and A_3AR preferentially couple to inhibitory G_i proteins, while A_{2A}AR and A_{2B}AR primarily couple to stimulatory G_s proteins to mediate intracellular signaling cascades (Fig. 6a). Structural comparisons reveal conformational differences between G_i- and G_s-coupled adenosine receptors complexes. Specifically, the TM6 helix of A_1AR/A_3AR-Gi complexes shows a 3.1 Å inward shift to accommodate G_i binding compared to A_{2A}AR/A_{2B}AR-G_s complexes (Fig. 6b). Additionally, the α5 helix of $G\alpha_s$ subunits displays a 8.6 Å displacement relative to its orientation in G_i complexes based on measurements of the Cα atom of $G\alpha^{H5.03}$ (Fig. 6c). The αN helix of $G\alpha_i$ exhibits a 3.3 Å tilt compared to G_s when measuring the Cα of $G\alpha^{HN.38}$ (Fig. 6d). Overall, the structural arrangements of A_1AR/A_3AR-G_i complexes closely resemble each other, similar to the consistency observed between A_{2A}AR/A_{2B}AR-G_s complexes. These findings reveal that G_i-coupled adenosine receptors adopt conserved G protein-binding conformations

that differ distinctly from those of G_s-coupled adenosine receptors. Elucidation of the structural differences governing adenosine receptors-G protein interactions provides fundamental insights into the molecular determinants of G protein coupling specificity.

Conclusion

In conclusion, we have determined the cryo-EM structures of the A_3AR bound to selective agonists CF101 and CF102 with heterotrimeric G_i protein. Despite the conserved binding of the core adenosine moiety, the structures revealed differences in the orientations of the N^6 substituted groups in CF101 and CF102. We identified ECL3 and key pocket residues $His^{3.37}$, $Ser^{5.42}$ and $Ser^{6.52}$ that confer selectivity over other adenosine receptor subtypes by mutagenesis studies. Comparison to an inactive A_{2A}AR structure provided insight into the conformational changes associated with A_3AR activation and G protein coupling. By elucidating the molecular mechanisms governing ligand recognition, signaling, and subtype selectivity, A_3AR structures significantly advance our fundamental understanding of this important drug target. The findings pave the way for structure-guided design of improved therapeutics targeting adenosine receptors for the treatment of cancer, inflammation, and other diseases.

Acknowledgements

We thanks Wen Hu, Kai Wu and Qingning Yuan from the Shanghai Advanced Center for Elecron Microscopy (Shanghai Institute of Materia Medica, Chinese Academy of Sciences) for their technical supporting and assistance with cryo-EM dataset collection. This project was supported by the CAS Strategic Priority Research Program (XDB37030103 to H.E.X.); Shanghai Municipal Science and Technology Major Project (H.E.X.); The National Natural Science Foundation of China (82121005 to X.X., Y.J., and H.E.X., 32130022 to H.E.X., 82330113 to X.X., 32301004 to H.C., 82304579 to S.G., and 32171187 to Y.J.); Shanghai Municipal Science and Technology Major Project (2019SHZDZX02 to H.E.X.); the Lingang Laboratory (LG-GG-202204-01 to H.E.X.); the National Key R&D Program of China (2018YFA0507002 to H.E.X.); China Postdoctoral Science Foundation (2021M703341, 2023T160662 to H.C.).

Author Contributions

H. C. designed the expression constructs, purified the protein complexes supervised by H.E.X.. Y.X. and H.C. prepared the grids and performed the cryo-EM data processing and model building with the help of J.L.. H.E.X., Y.J. and H.C. analyzed the structures. S.G. and Z.X. performed the functional studies with the help of J.S. under the supervision of X.X.. H.C. prepared the figures and manuscript. Y.X. and S.G. contributed to manuscript preparation. H.E.X. and H.C. wrote the manuscript with input from all authors.

Data availability

The atomic coordinates of CF101/CF102-A3AR-Gi complex have been deposited in the Protein Data Bank (http://www.rcsb.org) with accession codes xxxx and xxxx, respectively. The corresponding cryo-EM density maps have been deposited in the Electron Microscopy Data Bank (https://www.ebi.ac.uk/pdbe/emdb/) with accession codes EMD-xxxxx and EMD-xxxx, respectively.

Competing interests

The authors declare no competing interests.

References

1. Salvatore, CA, MA Jacobson, HE Taylor, J Linden and RG Johnson, Molecular cloning and characterization of the human A3 adenosine receptor. *Proc Natl Acad Sci U S A*, 1993. 90(21): 10365-9.
2. Sheth, S, R Brito, D Mukherjea, LP Rybak and V Ramkumar, Adenosine receptors: expression, function and regulation. *Int J Mol Sci*, 2014. 15(2): 2024-52.
3. Borea, PA, K Varani, F Vincenzi, PG Baraldi, MA Tabrizi, S Merighi and S Gessi, The A3 adenosine receptor: history and perspectives. *Pharmacol Rev*, 2015. 67(1): 74-102.
4. Jacobson, KA, S Merighi, K Varani, PA Borea, S Baraldi, M Aghazadeh Tabrizi, R Romagnoli, PG Baraldi, et al., A(3) Adenosine Receptors as Modulators of Inflammation: From Medicinal Chemistry to Therapy. *Med Res Rev*, 2018. 38(4): 1031-1072.
5. Hauser, AS, AJ Kooistra, C Munk, FM Heydenreich, DB Veprintsev, M Bouvier, MM Babu and DE Gloriam, GPCR activation mechanisms across classes and macro/microscales. *Nat Struct Mol Biol*, 2021. 28(11): 879-888.
6. Fishman, P, S Bar-Yehuda, BT Liang and KA Jacobson, Pharmacological and therapeutic effects of A3 adenosine receptor agonists. *Drug Discov Today*, 2012. 17(7-8): 359-66.
7. Fishman, P, S Bar-Yehuda, L Madi and I Cohn, A3 adenosine receptor as a target for cancer therapy. *Anticancer Drugs*, 2002. 13(5): 437-43.
8. Marwein, S, B Mishra, UC De and PC Acharya, Recent Progress of Adenosine Receptor Modulators in the Development of Anticancer Chemotherapeutic Agents. *Curr Pharm Des*, 2019. 25(26): 2842-2858.
9. Fishman, P, Drugs Targeting the A3 Adenosine Receptor: Human Clinical Study Data. *Molecules*, 2022. 27(12).
10. Jacobson, KA, Adenosine A3 receptors: novel ligands and paradoxical effects. *Trends Pharmacol Sci*, 1998. 19(5): 184-91.
11. Jacobson, KA, AM Klutz, DK Tosh, AA Ivanov, D Preti and PG Baraldi, Medicinal chemistry of the A3 adenosine receptor: agonists, antagonists, and receptor engineering. *Handb Exp Pharmacol*, 2009(193): 123-59.
12. Barkan, K, P Lagarias, M Stampelou, D Stamatis, S Hoare, D Safitri, KN Klotz, E Vrontaki, et al., Pharmacological characterisation of novel adenosine A(3) receptor antagonists. *Sci Rep*, 2020. 10(1): 20781.
13. Gallo-Rodriguez, C, XD Ji, N Melman, BD Siegman, LH Sanders, J Orlina, B Fischer, Q Pu, et al., Structure-activity relationships of N6-benzyladenosine-5'-uronamides as A3-selective adenosine agonists. *J Med Chem*, 1994. 37(5): 636-46.
14. Kim, HO, XD Ji, SM Siddiqi, ME Olah, GL Stiles and KA Jacobson, 2-Substitution of N6-benzyladenosine-5'-uronamides enhances selectivity for A3 adenosine receptors. *J Med Chem*, 1994. 37(21): 3614-21.
15. Van Schaick, EA, KA Jacobson, HO Kim, IJ AP and M Danhof, Hemodynamic effects and histamine release elicited by the selective adenosine A3 receptor agonist 2-Cl-IB-MECA in conscious rats. *Eur J Pharmacol*, 1996. 308(3): 311-4.
16. Suresh, RR, S Jain, Z Chen, DK Tosh, Y Ma, MC Podszun, Y Rotman, D Salvemini, et al., Design and in vivo activity of A(3) adenosine receptor agonist prodrugs. *Purinergic Signal*, 2020. 16(3): 367-377.

17. Fishman, P, S Cohen, I Itzhak, J Amer, A Salhab, F Barer and R Safadi, The A3 adenosine receptor agonist, namodenoson, ameliorates non‐alcoholic steatohepatitis in mice. *Int J Mol Med*, 2019. 44(6): 2256-2264.
18. Jacobson, KA and ZG Gao, Adenosine receptors as therapeutic targets. *Nat Rev Drug Discov*, 2006. 5(3): 247-64.
19. Verzijl, D and AP Ijzerman, Functional selectivity of adenosine receptor ligands. *Purinergic Signal*, 2011. 7(2): 171-92.
20. Duan, J, DD Shen, XE Zhou, P Bi, QF Liu, YX Tan, YW Zhuang, HB Zhang, et al., Cryo-EM structure of an activated VIP1 receptor-G protein complex revealed by a NanoBiT tethering strategy. *Nat Commun*, 2020. 11(1): 4121.
21. Cai, H, Y Xu, S Guo, X He, J Sun, X Li, C Li, W Yin, et al., Structures of adenosine receptor A(2B)R bound to endogenous and synthetic agonists. *Cell Discov*, 2022. 8(1): 140.
22. Duan, J, H Liu, F Zhao, Q Yuan, Y Ji, X Cai, X He, X Li, et al., GPCR activation and GRK2 assembly by a biased intracellular agonist. *Nature*, 2023. 620(7974): 676-681.
23. Lebon, G, T Warne, PC Edwards, K Bennett, CJ Langmead, AG Leslie and CG Tate, Agonist-bound adenosine A2A receptor structures reveal common features of GPCR activation. *Nature*, 2011. 474(7352): 521-5.
24. Draper-Joyce, CJ, R Bhola, J Wang, A Bhattarai, ATN Nguyen, I Cowie-Kent, K O'Sullivan, LY Chia, et al., Positive allosteric mechanisms of adenosine A(1) receptor-mediated analgesia. *Nature*, 2021. 597(7877): 571-576.
25. Tosh, DK, CL Fisher, V Salmaso, TC Wan, RG Campbell, E Chen, ZG Gao, JA Auchampach, et al., First Potent Macrocyclic A(3) Adenosine Receptor Agonists Reveal G-Protein and beta-Arrestin2 Signaling Preferences. *ACS Pharmacol Transl Sci*, 2023. 6(9): 1288-1305.
26. Jaakola, VP, MT Griffith, MA Hanson, V Cherezov, EY Chien, JR Lane, AP Ijzerman and RC Stevens, The 2.6 angstrom crystal structure of a human A2A adenosine receptor bound to an antagonist. *Science*, 2008. 322(5905): 1211-7.
27. Zhou, Q, D Yang, M Wu, Y Guo, W Guo, L Zhong, X Cai, A Dai, et al., Common activation mechanism of class A GPCRs. *Elife*, 2019. 8.
28. Mazziotta, C, JC Rotondo, C Lanzillotti, G Campione, F Martini and M Tognon, Cancer biology and molecular genetics of A(3) adenosine receptor. *Oncogene*, 2022. 41(3): 301-308.

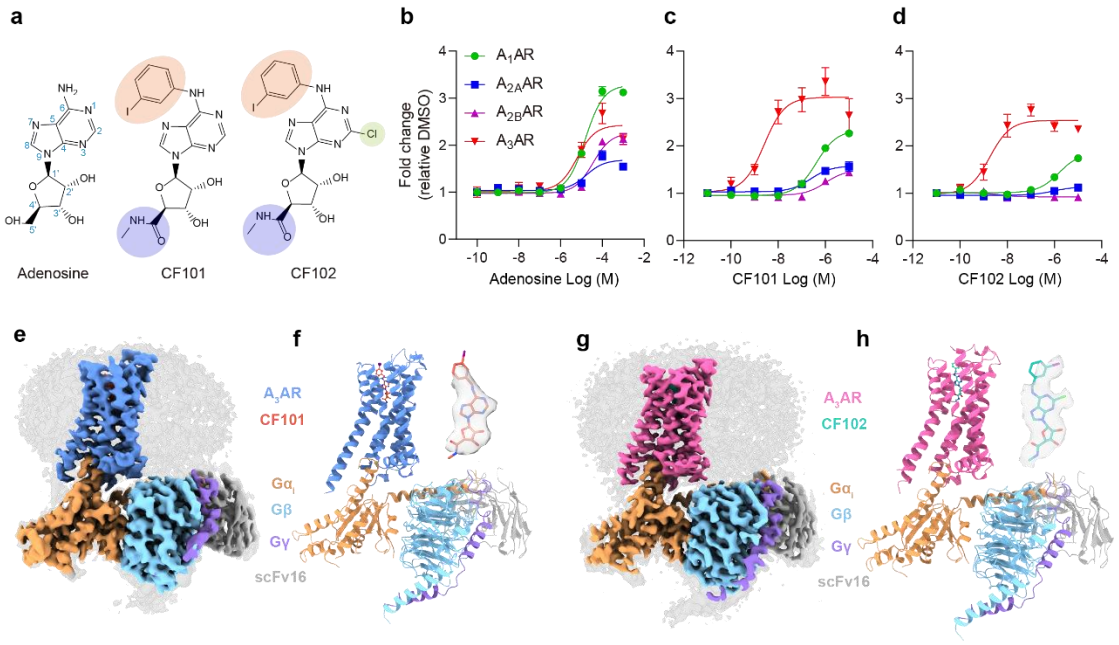

Fig 1. Cryo-EM structures of CF101-A_3AR-G_i and CF102-A_3AR-G_i complexes.

a. Chemical structures of the adenosine, CF101 and CF102. Highlighting modifications at the 5'-N-methylcarboxamide in the ribose group and N^6 and C2 positions of the adenoisine group. The atom numbering was indicated in blue. CF101, is also named IB-MECA and N^6-(3-iodobenzyl)adenosine-5'-N-methyluronamide. CF102, is also named Cl-IB-MECA and 2-chloro-N^6-(3-iodobenzyl)adenosine-5'-N-methyluronamide. **b-d.** NanoBiT association assays monitoring ligand activity on adenosine receptors for adenosine (**b**), CF101 (**c**) and CF102 (**d**) from three independent experiments in triplicate (n=3). **e, f.** Cryo-EM map (**e**) and model (**f**) of the CF101-A_3AR-G_i complex, with inset showing CF101 density. The density map in the inset is shown at 0.232 threshold. **g, h.** Cryo-EM map (**g**) and model (**h**) of the CF102-A_3AR-G_i complex, with inset showing CF102 density. The density map in the inset is shown at 0.17 threshold. Subunits are colored as indicated.

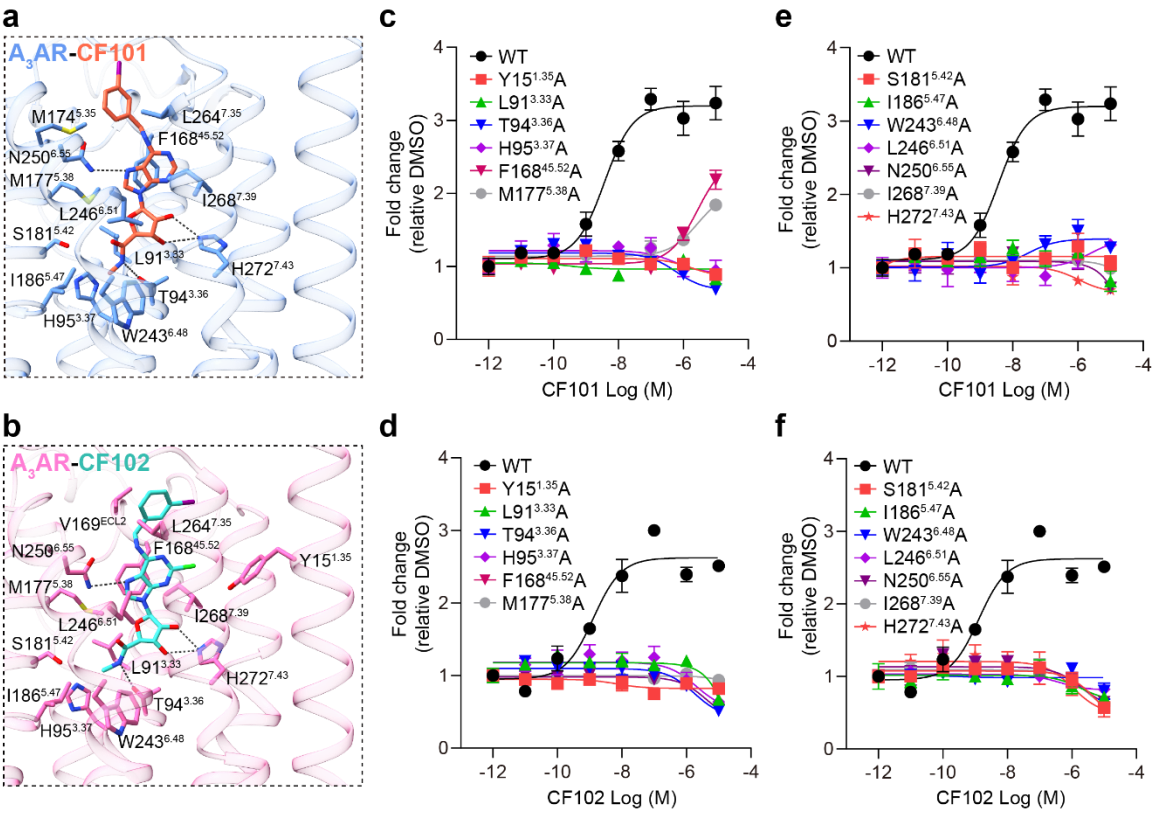

Fig 2. The orthosteric binding pocket.

a, b Detailed interactions between A_3AR and CF101 (**a**) or CF102 (**b**) from the membrane plane. Residues involved in ligand interaction are colored blue and pink in two complexes, respectively. Black dashed lines indicate hydrogen bonds. **c-f** Dose-response curves of muntants of A_3AR induced by CF101 (upper panels, **c**, **e**) or CF102 (lower panels, **d**, **f**) using NanoBiT assay.

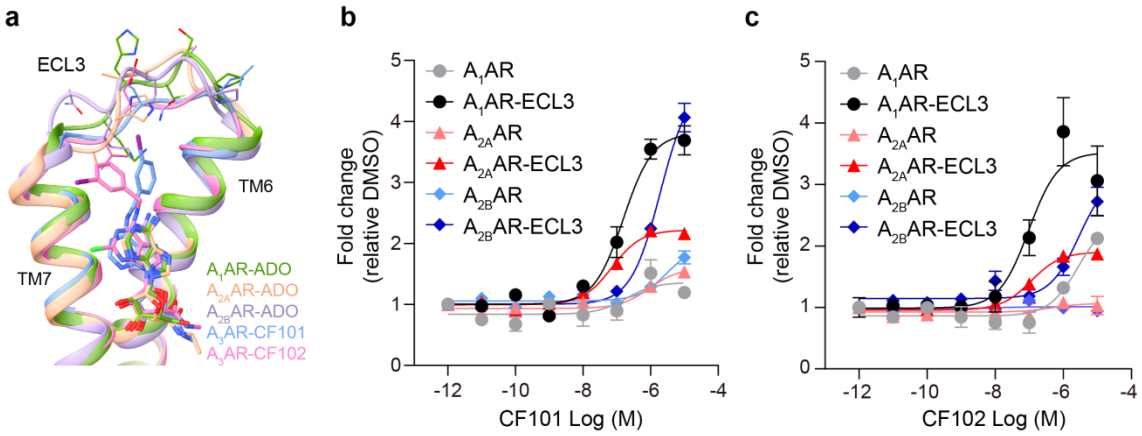

Fig 3. Swapping ECL3 increases CF101/CF102 potency at adenosine A_1/A_{2A}/A_{2B} receptor subtypes.

a Superposition of ECL3 in the adenosine receptors shows A_3AR reveals A_3AR has a shorter ECL3. Other TMs were omitted. **b, c** Effects of CF101 and CF102 were tested on the A_1AR, A_{2A}AR, and A_{2B}AR and their corresponding mutants containing the swapped ECL3 from the A_3AR using NanoBiT assays.

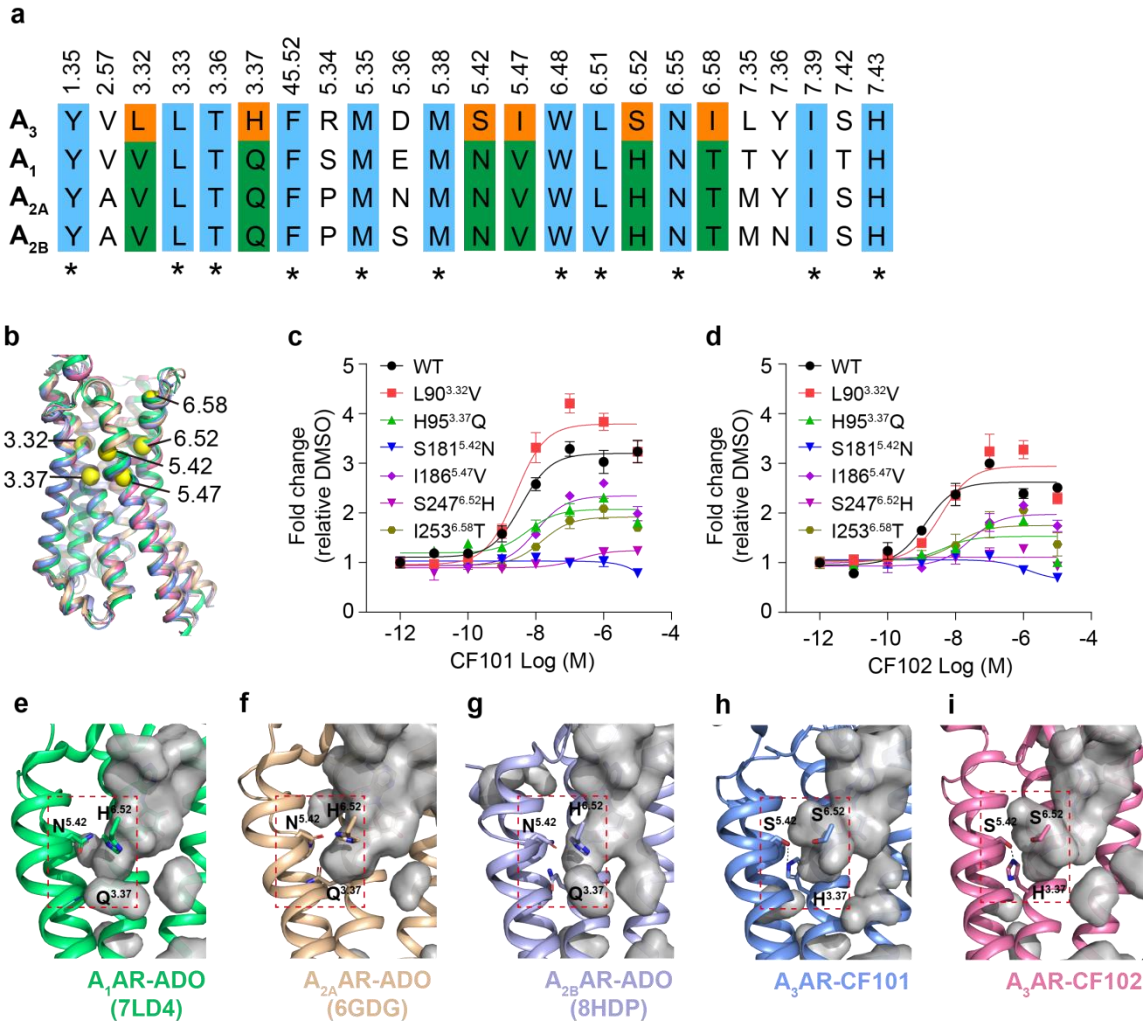

Fig 4. Key residues in the A_3AR binding pocket.

a Sequence alignment of the residues in the orthosteric binding pocket among the adenosine receptors. The conserved residues were colored with blue and stars marked. The unique residues in A_3AR, different from other adenosine receptors subtypes were colored in orange, while the others subtpyes at corresponding position were colored in green. All residues were annotated based on GPCR Ballesteros-Weinstein numbering scheme. **b** Superposition of adenosine receptors, the unique residues in A_3AR from the other adenosine receptors are shown as yellow ball. **c-d** Effects of CF101/CF102 on A_3AR mutants containing swapped residues from other adenosine receptors by NanoBiT assay. **e-i** The binding cavities of the adenosine receptors are generated in PyMOL, the cavities were depicted as gray. In A_3AR, $His^{3.37}$,$Ser^{5.42}$ and $Ser^{6.52}$ form a subpocket, whereas these positions are conserved as $Gln^{3.37}$, $Asn^{5.42}$ and $His^{6.52}$ in the other adenosine receptor subtypes, respectively (His, H; Ser, S; Gln, Q; Asn, N). Dash lines in **h** and **i** showed the hydrogen bonds between $His^{3.37}$ and $Ser^{5.42}$.

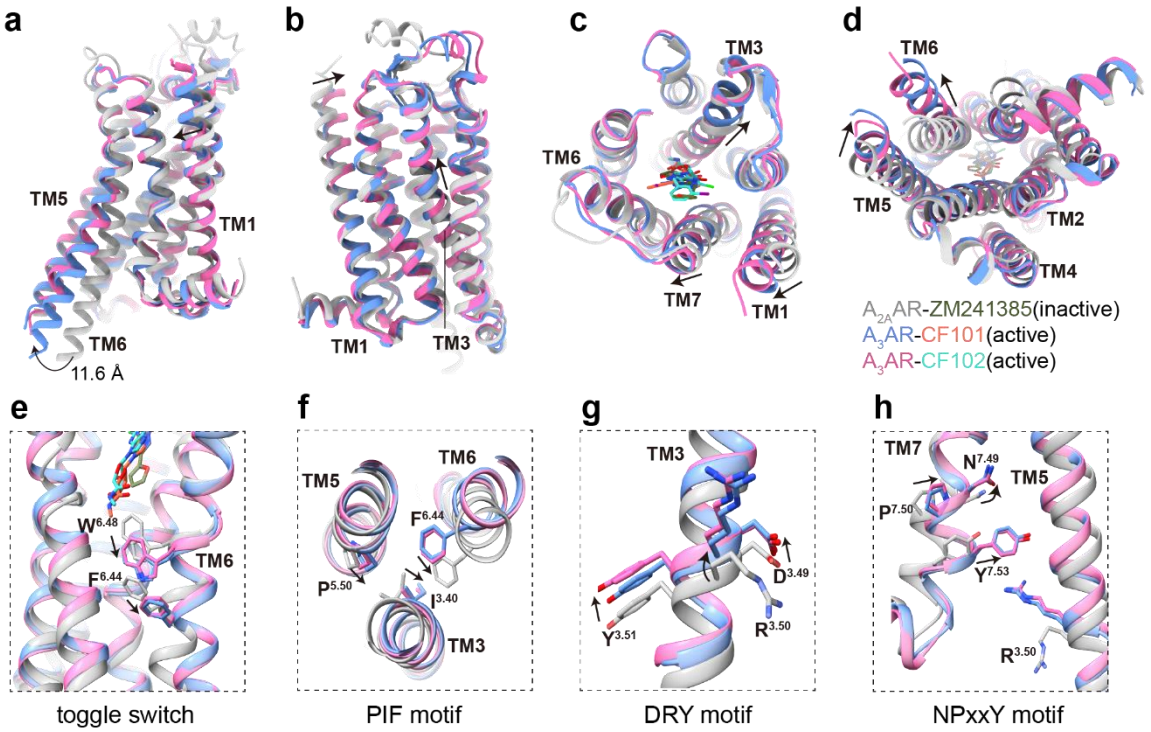

Fig 5. A_3AR activation mechanism.

a-b Superposition of active A_3AR-CF101/CF102 complexes (blue/pink) with inactive A_{2A}AR-ZM241385 complex (grey, PDB ID 4EIY). **c,d** Comparison of extracellular (**c**) and cytoplasmic (**d**) views of active A_3AR and inactive A_{2A}AR. **e-g** Conformational changes in conserved motifs, including toggle switch, PIF, DRY and NPxxY, upon CF101/CF102 binding to A_3AR relative to inactive A_{2A}AR-ZM241385. Arrows indicate movement directions.

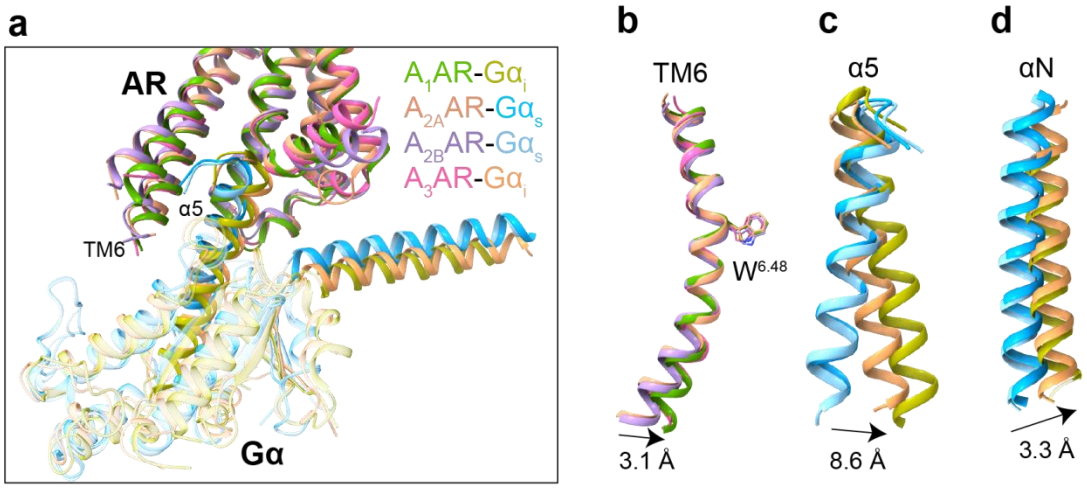

Figure 6. G protein coupling of adenosine receptors.

a Comparison of G protein conformations in A_1/A_3AR-G_i and A_{2A}/A_{2B}AR-G_s complexes. **b** Conformational comparison of TM6 in adenosine receptors, referencing toggle switch $W^{6.48}$ in TM6 of receptor. **c-d** Conformational comparison of α5 helix and αN helix in G protein adenosine receptors-G protein complexes. Arrows indicate movement directions.

Methods

Construct design

The full-length gene coding human A_3AR was synthesized (Synbio) and subcloned into pFastBac vector using CloneExpress II one step cloning kit (Vazyme Biotech). A hemagglutinin signal peptide and thermostabilized apocytochrome b562RIL (BRIL) were fused at the N-terminal of A_3AR to enhance receptor expression. To enhance complex stability, a NanoBiT tethering approach was used where an LgBiT domain was fused to the C-terminal of the receptor[20]. A dual maltose-binding protein was linked after LgBiT through a tobacco etch virus protease site (TEV site) for further cleavage. A dominant-negative mutant of bovine $G\alpha_i$ containing G203A/A326S[29] mutations was generated to stabilize the heterotrimeric $G\alpha_i\beta\gamma$ protein. Rat Gβ1 was fused with a HiBiT at C-terminal for structural complementation of LgBiT to form a NanoBiT. The single-chain variable fragement scFv16 was applied to bind the $G\alpha_i\beta\gamma$ protein for stabilization[30]. $G\alpha_i$, Gβ1-HiBiT, Gγ, and scFv16, were cloned into pFastBac vector (Supplementary Fig. 1a), respectively.

Protein expression and purification

The recombinant A_3AR, $G\alpha_i$, Gβ1-HiBiT, Gγ, and scFv16 were co-expresed in *Trichoplusia ni* High Five insect cells using the Bac-to-Bac baculovirus expression system. High Five cells was co-infected with the baculovirus at a cell density of 3.5×10^6 cells per milliliter. Fourty-eight hours later, the infected cells were harvested and stored at -80 °C until used.

For the purification of the CF101-A_3AR-G_i complex, cells pellets was thawed and resuspended in Buffer A (100 mM NaCl, 20 mM HEPES, pH 7.5) supplemented with protease inhibitor cocktail (TargetMol). Cells was lysed by dounce homogenization followed by centrifugation to remove unsoluble materials. The pellets were responded in Buffer B (100 mM NaCl, 10 %(v/v) glycerol, 20 mM HEPES, pH7.5) supplemented with 10 mM $MgCl_2$, 5 mM $CaCl_2$, 0.2 mM Tris-(2-carboxyethyl)phosphine (TCEP, Hampton Research) and protease inhibitor cocktail. The complex was formed by rotating at room temperature for 1 h after addition of 25 mU/mL apyrase and 10 μM CF101. After incubation, the sample was solubliezed in 0.5 %(w/v) lauryl maltose neopentylglycol (LMNG, Anatrace) and 0.1%(w/v) cholesteryl hemisucinate (CHS, Anatrace) for 3 h at 4 °C. The supernatant was clarified by centrifugation at 100,000× g for 40 min. The supernatant was incubated with dextrin beads 6FF (Smart-Lifescience) for 3 h at 4 °C. The beads were loaded onto a gravity column and washed with 20 column volumes of Buffer C (100 mM NaCl, 2 mM $MgCl_2$, 10 μM CF101, 0.2 mM TCEP, 0.01 %(w/v) LMNG, 0.002 %(w/v) CHS, 20 mM HEPES, pH 7.5). The complex was eluted with Buffer C supplemented with 10 mM maltose and further concentrated using 100 kDa molecular weight cut-off concentrator. TEV protease was added to the concentrated protein at 4 °C overnight to cleave dual maltose binding protein from fusion protein. After digestion, sample was loaded onto Superdex 200

Increase 10/300 GL column (GE Healthcare) with Buffer D (100 mM NaCl, 2 mM $MgCl_2$, 10 μM CF101, 0.1 mM TCEP, 0.00075 %(w/v) LMNG, 0.00025 %(w/v) glyco-diosgenin, 0.0002 %(w/v) CHS, 20 mM HEPES, pH 7.5). The desired fractions were pooled and concentrated to 5-8 mg/mL for cryo-EM sample preparation.

Cryo-EM data collection

Cryo-EM grids were prepared with the Vitrobot Mark IV plunger (FEI) set to 8 °C and 100% humidity. Three-microliters of the CF101-A_3AR-G_i complex were applied to glow- discharged Quantifoil R1.2/1.3 holey carbon grids. The sample was incubated for 10 s on the grids before blotting for 3.5 s (double-sided, blot force 1) and flash-frozen in liquid ethane immediately. The same conditions were used for the CF101-A_3AR-G_i complex sample.

For CF101-A_3AR-G_i complex, three datasets comprising 20,779 movies were collected on a Titan Krios equipped with a Gatan K3 direct electron detection device at 300 kV with a magnification of 105,000 corresponding to a pixel size 0.824 Å. Image acquisition was performed with EPU Software (FEI Eindhoven, Netherlands). We collected a total of 36 frames accumulating to a total dose of 50 e^- $Å^{-2}$ over 2.5 s exposure.

For CF102-A_3AR-G_i complex dataset, two datasets totaling 13,581 movies were collected on a Titan Krios equipped with a Gatan K3 detector at 300 kV with a magnification of 105,000 and pixel size of 0.824 Å, using EPU Software (FEI Eindhoven, Netherlands). Thirty-six frames were collected over a 2.5-s exposure to a dose of 50 e^- $Å^{-2}$.

Image processing

MotionCor2 was used to perform the frame-based motion-correction algorithm to generate drift-corrected micrograph for further processing, and CTFFIND4 provided estimation of contrast transfer function (CTF) parameters[31, 32].

For the CF101-A_3AR-G_i dataset, the previously resolved structure of BAY 60-6583-A_{2B}AR-G_s [21] was used as a reference for automatic particle picking in Relion 3.0[33]. Particle picking and extraction yielded 4,550,294 particles after 2D classification clearance, which were imported into cryoSPARC[34]. Four rounds of 2D classification selected 1,267,837 particles, followed by two rounds of 3D heterogenous refinement giving 982,833 particles. After two additional rounds of 2D classification and two rounds of heterogenous refinement, 271,323 particles were refined to a structure at 3.29 Å global resolution using non-uniform refinement (Supplementary Fig. 2).

For CF102-A_3AR-G_i complex dataset, the BAY 60-6583-A_{2B}AR-G_s structure[21] was again used for reference-based particle picking. 4,090,959 and 4,833,382 particles were autopicked and extracted from Dataset1 and Dateset2, respectively. For Dataset1, two rounds of 2D classification were used to separate out 1,070,085 particles. Masked 3D classification on the receptor part was used to separate out 175,747 particles that resulted to a clearer density of A_3AR. For Dataset2, two rounds of 2D classification and two rounds of 3D classification were performed to separate out 246,392 particles. After clearance, the remained particles from two datasets were combined and subjected to alignment-free 3D classification. 283,561 particles were remained and transferred in cryoSPARC[34]. One round of heterogenous refinement yielded a final 102,581 particle were refined to a structure at 3.19 Å global resolution using non-uniform refinement (Supplementary Fig. 3).

Model building

An A_3AR structure predicted by AlphaFold2 was used as the starting reference models for receptors building[35]. Structures of $G\alpha_i$, Gβ, Gγ and the scFv16 were derived from PDB entry 7EZH[36] were rigid body fit into the density. All models were fitted into the EM density map using UCSF Chimera[37] followed by iterative rounds of manual adjustment and automated rebuilding in COOT[38] and PHENIX[39], respectively. The model was finalized by rebuilding in ISOLDE[40] followed by refinement in PHENIX with torsion-angle restraints to the input model. The final model statistics were validated using Comprehensive validation (cryo-EM) in PHENIX and provided in the supplementary information, Supplementary Table 1. All structural figures were prepared using Chimera[37], Chimera X[41], and PyMOL (Schrödinger, LLC.).

NanoBiT assay

To monitor G protein interaction with A_1AR, A_{2A}AR, A_{2B}AR or A_3AR upon agonist stimulation, a NanoLuc-based NanoBiT enzyme complementation assay was used (Promega). The C-terminus of A_1AR, A_{2A}AR or A_{2B}AR was fused to SmBiT, while LgBiT was fused to the N-terminus of G proteins. The C terminus of A_3AR was fused with LgBiT, and the SmBiT element was fused to the N terminus of G proteins. HEK293 cells were seeded at 4×10^4 cells/well on 96-well plates and co-transfected with AR-SmBit and LgBiT-G protein plasmids at a 1:1 mass ratio. After 24 hours, cells were replaced with 40 μL fresh culture medium without fetal bovine serum. Ten microliter Nano-Glo Live Cell reagent was added followed the manufacturer's protocol (Promega, N2011), and incubated at 37 °C, 5 % CO_2 for 5 min. Another 25 μL culture medium containing various concentrations of compounds were added and incubated at room temperature for 10 minutes before measuring bioluminescence using EnVision multiplate reader (PerkinElmer).

Cell-surface expression assay

Wild type A_1AR, A_{2A}AR, A_{2B}AR or A_3AR gene was subcloned into pcDNA3.0 vector with an N-terminal human influenza hemagglutinin tag (HA-tag). HEK293 were seeded at 4×10^4 cells/well on 96-well plates and transfected with wild type (WT) or adenosine receptor mutants. After 24 hours, cells were washed with PBS buffer, fixed with 4 %(w/v) paraformaldehyde for 15 min, and blocked with 2 %(w/v) bovin serum albumin (BSA) for 1 h. Next, cells were incubated with the polyclonal anti-HA (Sigma, H6908) overnight at 4 °C, followed by 1 h with horseradish peroxidase (HRP)-conjugated anti-rabbit antibody (Cell Signaling, 7074S) at room temperature. After washing, 50 μL tetramethylbenzidine (Sigma, T0440) was added for 30 min before stopping the reaction with 25 μL TMB substrate stop solution (Beyotime, P0215). Absorbance at 450 nm was measured on a FlexStation III microplate reader (Molecular Devices).

Statistical analysis

All functional study data were analyzed in Prism 8 (GraphPad) and presented as means ± S.E.M. from at least three independent experiments. Concentration-response curves were evaluated with a three-parameter logistic equation. EC_{50} values were calculated using the sigmoid three-parameter equation. Significance was determined by one-way ANOVA followed by multiple comparisons test, and $^*P < 0.05$ *vs.* wild-type (WT) was considered statistically significant.

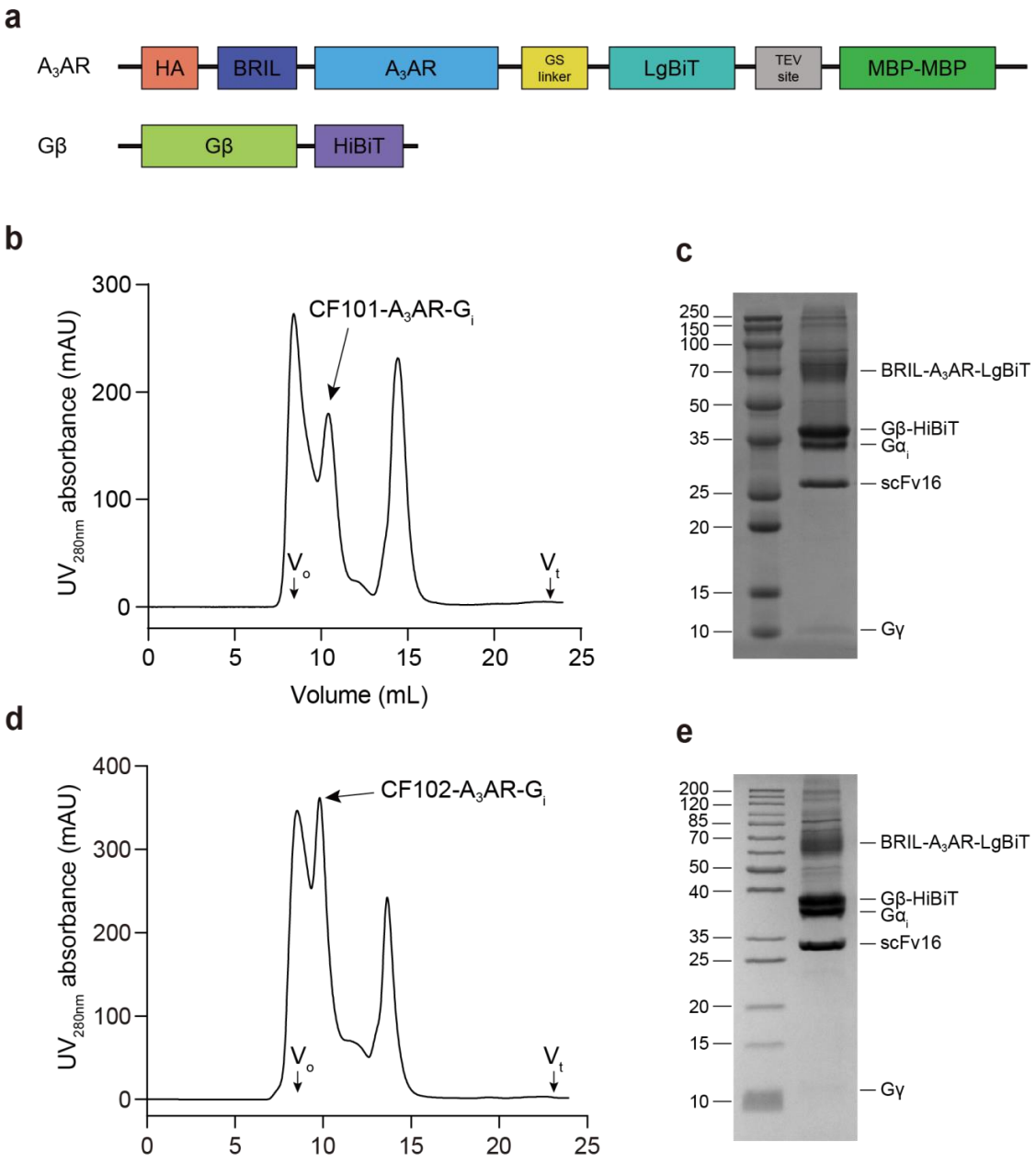

Supplementary Fig. 1 The expression and purification of A_3AR-G_i complex.
a. Schematic diagrams of the expression constructs of A_3AR and Gβ1 using the NanoBiT tethering approach. A_3AR and Gβ1 fused with LgBiT and HiBiT, respectively. **b.** Size-exclusion chromatography profile of the CF101-A_3AR-G_i complex. **c.** SDS-PAGE of the arrow indicated peak fraction in (**b**). **d.** Size-exclusion chromatography profile of the CF102-A_3AR-G_i complex. **e.** SDS-PAGE of the arrow indicated peak fraction in (**d**).

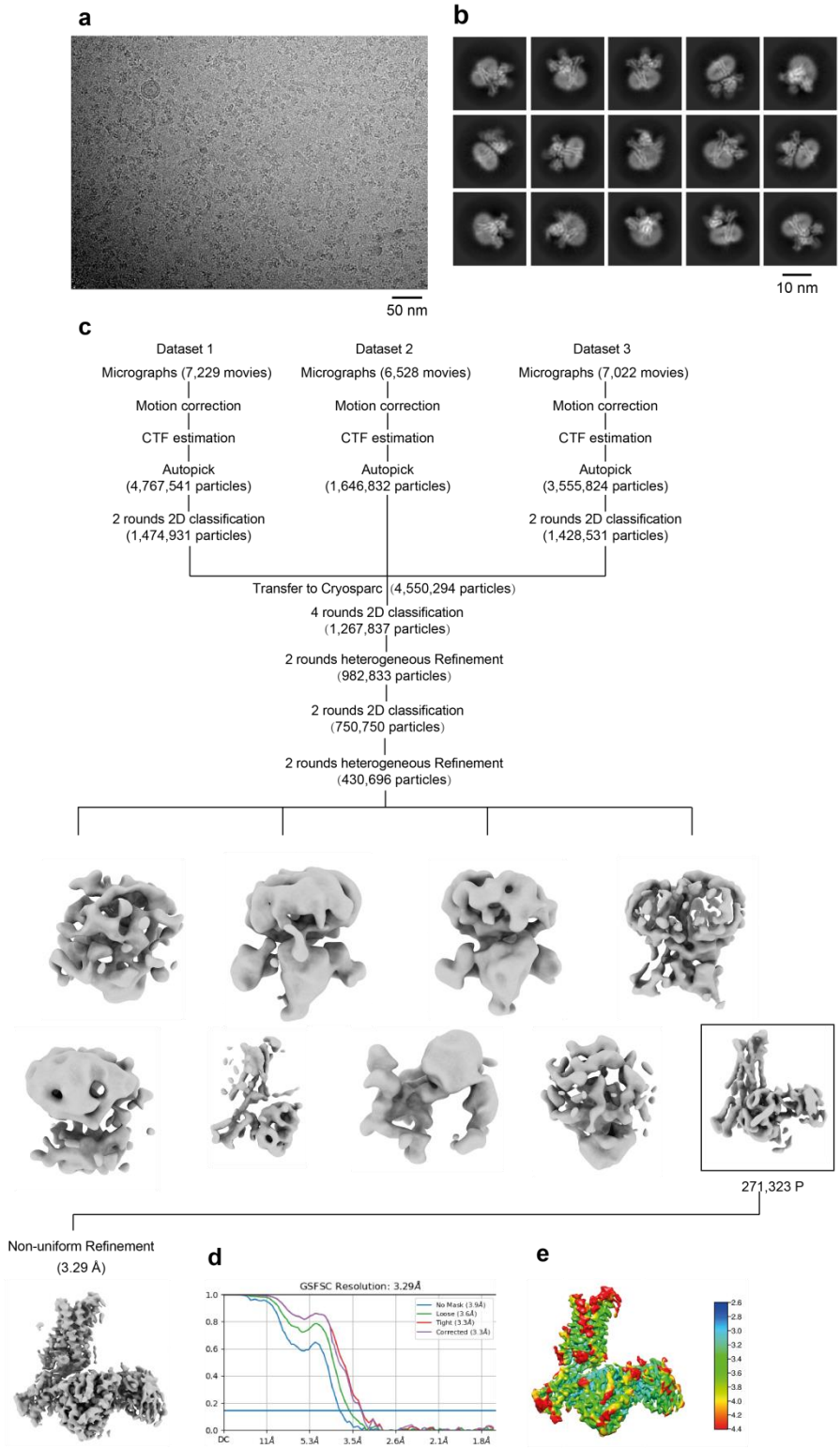

Supplementary Fig. 2 Cryo-EM data processing of CF101-A_3AR-G_i complex. **a.** Representative image from cryo-EM dataset. Scale bar, 50 nm. **b.** Respresentative 2D average classification classes. Scale bar, 10 nm. **c.** Flow-chart of the cryo-EM data processing. **d.** FSC curves. **e.** The local resolution map.

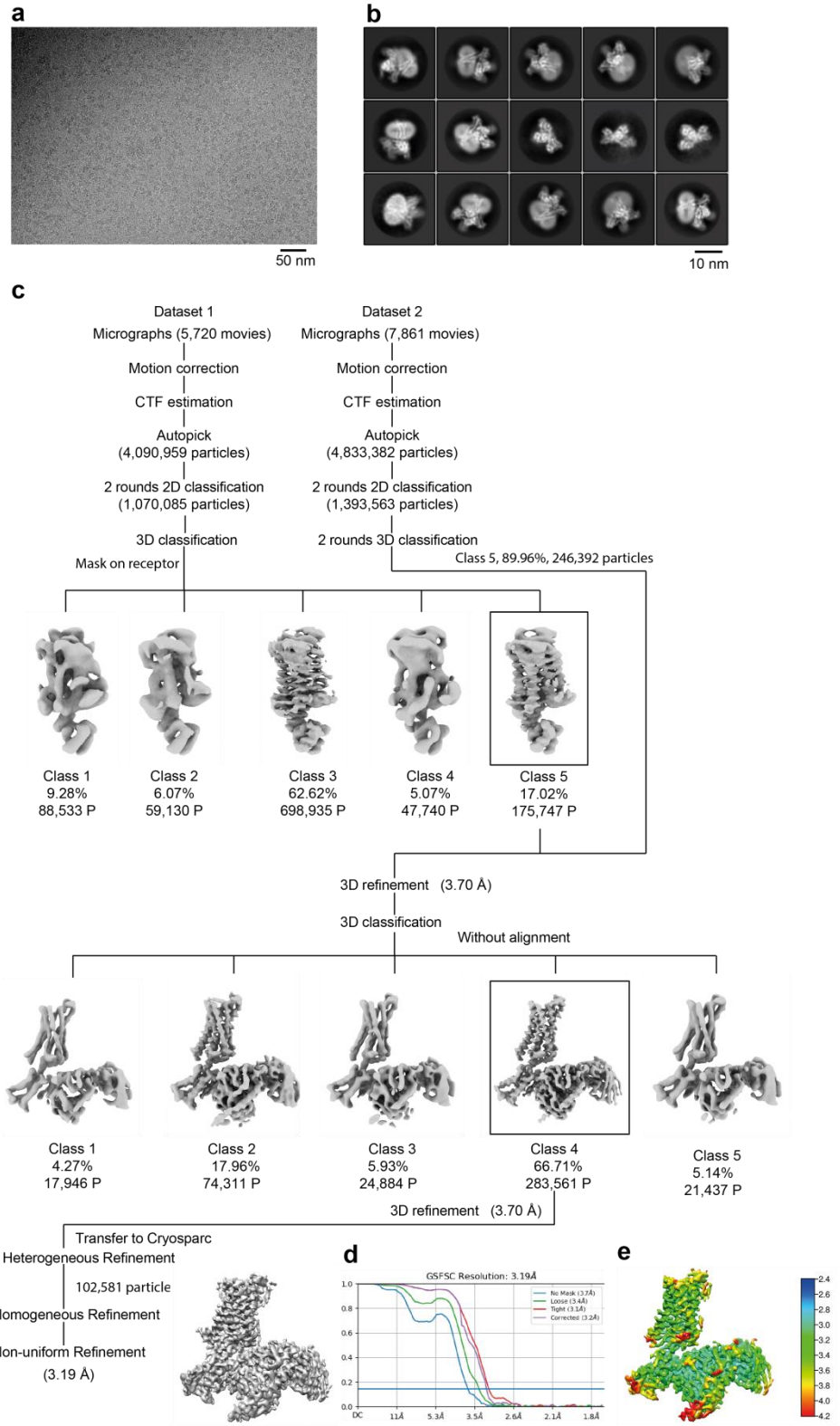

Supplementary Fig. 3 Cryo-EM data processing of CF102-A_3AR-G_i complex. **a.** Representative image from cryo-EM dataset. Scale bar, 50 nm. **b.** Respresentative 2D average classification classes. Scale bar, 10 nm. **c.** Flow-chart of the cryo-EM data processing. **d.** FSC curves. **e.** The local resolution map.

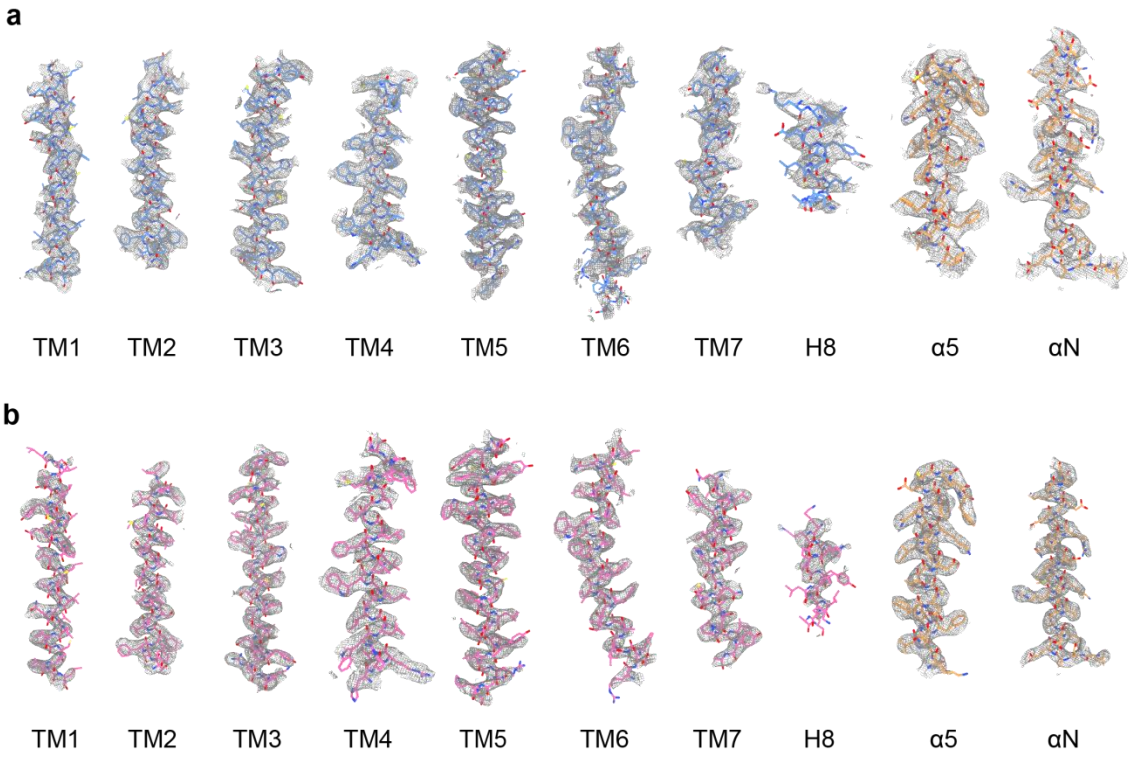

Supplementary Fig. 4 Respresentative regions of cryo-EM density maps are shown for the each transmembrane helical (TM) of A_3AR and the α5 and αN helices of $G\alpha_i$.

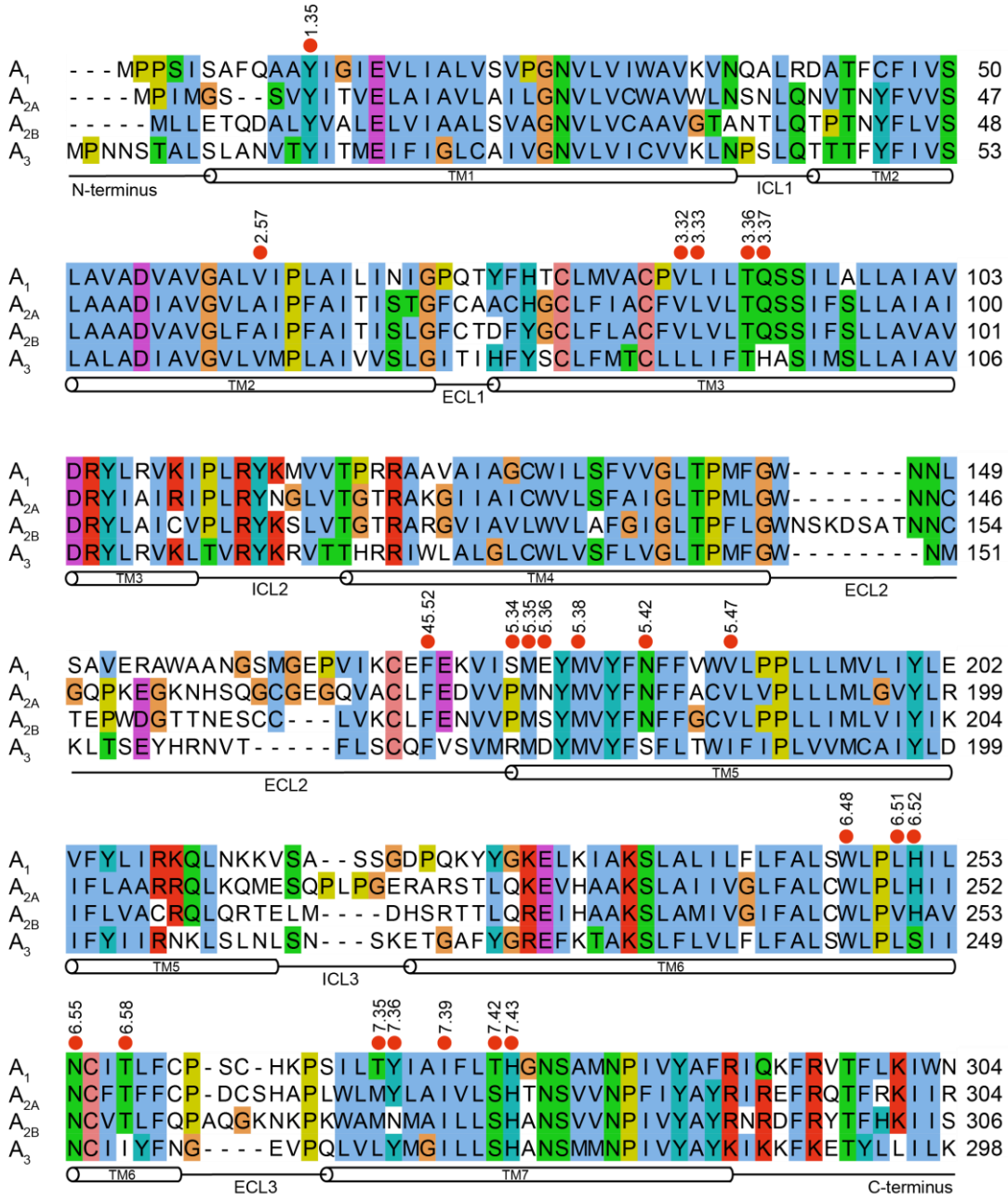

Supplementary Fig. 5 Sequence alignment of adenosine receptors. The sequence alignment was generated with Jalview[42] and depicts the N-/C-turminus, transmembrane helices (TMs), extracellular loops (ECLs), and intracellular loops (ICLs). Residues lining the orthosteric binding site are highlighted with red circles and annotated with GPCR Ballesteros-Weinstein numbering scheme. The C-terminus of the adenosine receptors were omitted.

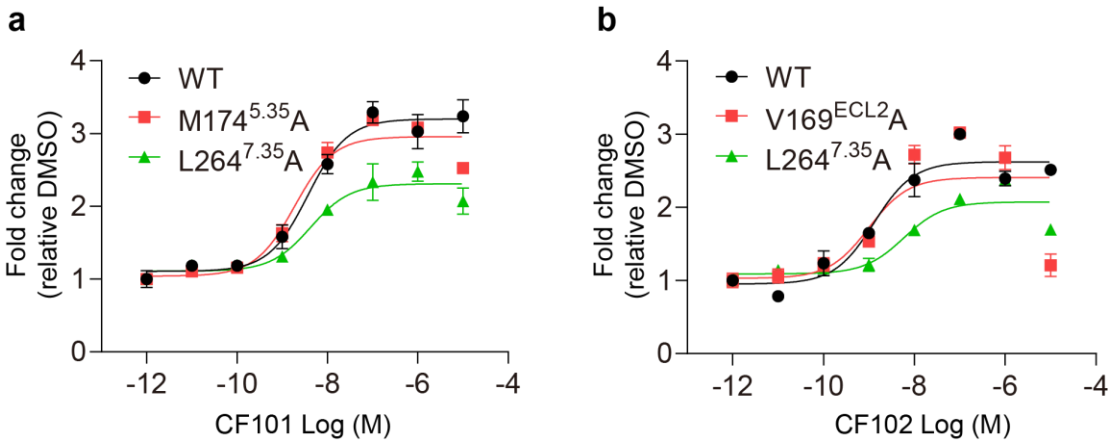

Supplementary Fig. 6 Effects of CF101 or CF102 on the A_3AR mutants. These residues in A_3AR formed hydrophobic interactions with the 3-iodophenyl group present in CF101 and CF102.

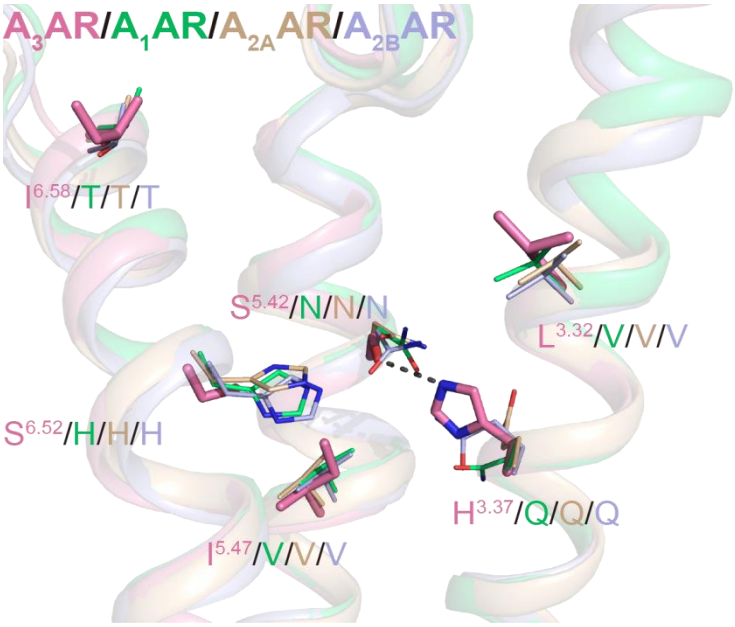

Supplementary Fig. 7 The orthosteric binding pockets among adenosine receptors. The positions highlighted indicate where unique residues occurred in A_3AR compared to other adenosine receptors. The receptor names and their associated colors are shown above the models. The side chains in A3AR were depicted as bold sticks, while the corresponding side chains in other adenosine receptors were shown as thick sticks.

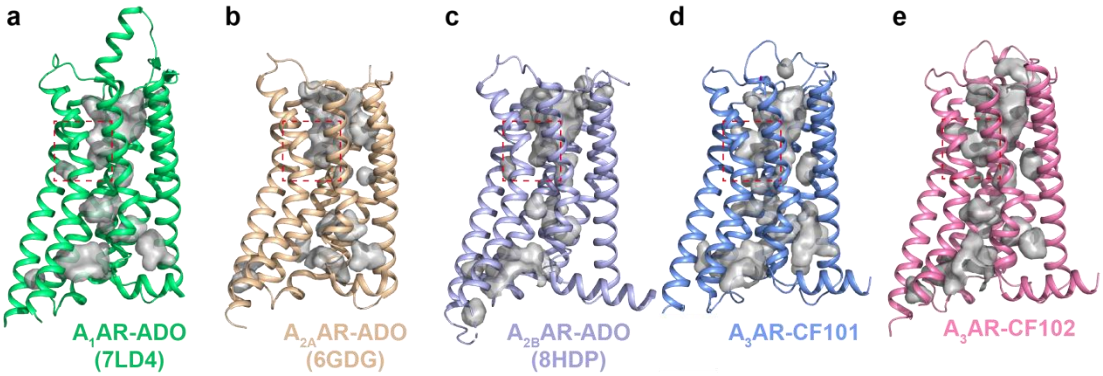

Supplementary Fig. 8 The binding cavities in adenosine receptors.

a-e The binding cavities of the adenosine receptors are depicted as gray surfaces, with the bound ligands shown as sticks. The receptor names and associated PDB codes[21, 24, 43] are indicated below each model. The unique subpocket in the A_3AR as the red boxes circled.

Supplementary Table 1 Cryo-EM data collection, model refinement and validation statistics.

	A_3AR-CF101-G_i complex	A_3AR-CF102-G_i complex
Data collection and processing		
Detector	K3	K3
Magnification	105,000	105,000
Voltage (kV)	300	300
Electron exposure ($e^-/Å^2$)	50	50
Defocus range (μm)	-1.0~-3.0	-1.0~-3.0
Pixel size (Å)	0.824	0.824
Symmetry imposed	C1	C1
Initial particle projections (no.)	9,970,197	8,924,341
Final particle projections (no.)	271,323	102,581
Map resolution (Å)	3.29	3.19
Map resolution range (Å)	2.60-4.40	2.40-4.20
FSC threshold	0.143	0.143
Model Refinement		
Refinement package	PHENIX-1.17.1-3660	PHENIX-1.17.1-3660
Real or reciprocal space	Real space	Real space
Model-Map CC (mask)	0.60	0.72
Model resolution (Å)	4.10	3.40
FSC threshold	0.5	0.5
B factors ($Å^2$, min/max/mean value)		
Protein residues	30.00/127.38/68.24	30.00/135.93/68.27
Ligands	20.00/20.00/20.00	20.00/20.00/20.00
Model composition		
Non-hydrogen atoms	8,751	8,753
Protein residues	1,126	1,127
R.m.s. deviations		
Bond lengths (Å)	0.001	0.005
Bond angles (°)	0.398	0.900
Validation		
MolProbity score	1.46	1.15
Clashscore	8.51	3.62
Rotamer outliers (%)	0.00	0.00
Ramachandran plot		
Favored (%)	98.19	98.38
Allowed (%)	1.81	1.62
Disallowed (%)	0.00	0.00
Data availability		
EMDB code		
PDB code		

Supplementary Table 2 Cell surface expression of A_3AR and its mutants on CF101- and CF102-induced NanoBiT assay.

	EC_{50} (nM)[a]		Cell-surface expression (Relative to WT)[a]
	CF101	CF102	
WT	3.74±0.7	1.50±0.4	100±2.5
$Y15^{1.35}A$	UD[b]	UD	113±5.0
$L90^{3.32}V$	2.71±0.6	3.94±0.5	79.6±6.8
$L91^{3.33}A$	UD	UD	107±12.1
$T94^{3.36}A$	UD	UD	91.5±4.7
$H95^{3.37}A$	UD	UD	121±7.1
$H95^{3.37}Q$	7.70±3.9	5.01±1.6	124±5.6*
$F168^{ECL2}A$	>10000	UD	116±4.0
$V169^{ECL2}A$	NT[c]	1.07±0.3	85.9±6.0
$M174^{5.35}A$	1.973±0.5	NT	85.0±2.3
$M177^{5.38}A$	>10000	UD	110±1.4
$S181^{5.42}A$	UD	UD	102±5.3
$S181^{5.42}N$	UD	UD	88.8±4.1
$I186^{5.47}A$	UD	UD	79.2±2.7
$I186^{5.47}V$	10.64±2.3	29.96±7.1***	93.6±2.3
$W243^{6.48}A$	>10000	UD	65.5±6.2***
$L246^{6.51}A$	>10000	UD	81.0±4.9
$S247^{6.52}H$	>10000	UD	82.5±6.2
$N250^{6.55}A$	UD	UD	78.2±5.0
$I253^{6.58}T$	17.04±4.1**	13.11±4.5	90.1±9.8
$L264^{7.35}A$	4.08±0.8	5.53±1.5	73.7±3.8*
$I268^{7.39}A$	UD	UD	67.4±4.2**
$H272^{7.43}A$	UD	UD	12.7±3.6***

[a] Data shown are means ± S.E.M. from at least three independent experiments.

[b] UD indicates that the activation level is too low to determine EC_{50} values.

[c] NT, not test.

* P<0.01; ** P<0.001 and *** P<0.0001 by one-way ANOVA followed by multiple comparisons test, compared with WT.

Supplementary Table 3 Cell surface expression of $A_1AR/A_{2A}AR/A_{2B}AR$ and its relative mutant on CF101- and CF102-induced NanoBiT assay.

Receptor	CF101		CF102		Cell-surface expression (Relative to WT) [a]
	EC_{50} (nM) [a]	max change (Relative to basal) [a]	EC_{50} (nM)	max change (Relative to basal)	
A_1AR	206.8±55	1.19±0.1	>10000	2.12±0.1	100±1.5
A_1AR-ECL3	161.9±36	3.69±0.2***	176.6±102	3.86±0.6**	91.1±3.2
$A_{2A}AR$	1280±727	1.53±0.1	UD[b]	1.03±0.1	100±2.9
$A_{2A}AR$-ECL3	74.29±16	2.21±0.1*	48.04±28	1.84±0.1	92.1±1.6
$A_{2B}AR$	>10000	1.77±0.1	UD	0.95±0.1	100±7.6
$A_{2B}AR$-ECL3	1952±289	4.06±0.2***	>10000	2.72±0.2**	80.5±1.9**

[a] Data shown are means ± S.E.M. from at least three independent experiments.

[b] UD indicates that the activation level is too low to determine EC_{50} values.

* P<0.01; ** P<0.001 and *** P<0.0001 by one-way ANOVA followed by multiple comparisons test, compared with WT.

References

20. Duan, J, DD Shen, XE Zhou, P Bi, QF Liu, YX Tan, YW Zhuang, HB Zhang, et al., Cryo-EM structure of an activated VIP1 receptor-G protein complex revealed by a NanoBiT tethering strategy. *Nat Commun*, 2020. 11(1): 4121.
21. Cai, H, Y Xu, S Guo, X He, J Sun, X Li, C Li, W Yin, et al., Structures of adenosine receptor A(2B)R bound to endogenous and synthetic agonists. *Cell Discov*, 2022. 8(1): 140.
24. Draper-Joyce, CJ, R Bhola, J Wang, A Bhattarai, ATN Nguyen, I Cowie-Kent, K O'Sullivan, LY Chia, et al., Positive allosteric mechanisms of adenosine A(1) receptor-mediated analgesia. *Nature*, 2021. 597(7877): 571-576.
29. Liu, P, MZ Jia, XE Zhou, PW De Waal, BM Dickson, B Liu, L Hou, YT Yin, et al., The structural basis of the dominant negative phenotype of the Galphai1beta1gamma2 G203A/A326S heterotrimer. *Acta Pharmacol Sin*, 2016. 37(9): 1259-72.
30. Maeda, S, A Koehl, H Matile, H Hu, D Hilger, GFX Schertler, A Manglik, G Skiniotis, et al., Development of an antibody fragment that stabilizes GPCR/G-protein complexes. *Nat Commun*, 2018. 9(1): 3712.
31. Rohou, A and N Grigorieff, CTFFIND4: Fast and accurate defocus estimation from electron micrographs. *J Struct Biol*, 2015. 192(2): 216-21.
32. Zheng, SQ, E Palovcak, JP Armache, KA Verba, Y Cheng and DA Agard, MotionCor2: anisotropic correction of beam-induced motion for improved cryo-electron microscopy. *Nat Methods*, 2017. 14(4): 331-332.
33. Zivanov, J, T Nakane, BO Forsberg, D Kimanius, WJ Hagen, E Lindahl and SH Scheres, New tools for automated high-resolution cryo-EM structure determination in RELION-3. *Elife*, 2018. 7.
34. Punjani, A, JL Rubinstein, DJ Fleet and MA Brubaker, cryoSPARC: algorithms for rapid unsupervised cryo-EM structure determination. *Nat Methods*, 2017. 14(3): 290-296.
35. Jumper, J, R Evans, A Pritzel, T Green, M Figurnov, O Ronneberger, K Tunyasuvunakool, R Bates, et al., Highly accurate protein structure prediction with AlphaFold. *Nature*, 2021. 596(7873): 583-589.
36. Liu, Q, D Yang, Y Zhuang, TI Croll, X Cai, A Dai, X He, J Duan, et al., Ligand recognition and G-protein coupling selectivity of cholecystokinin A receptor. *Nat Chem Biol*, 2021. 17(12): 1238-1244.
37. Pettersen, EF, TD Goddard, CC Huang, GS Couch, DM Greenblatt, EC Meng and TE Ferrin, UCSF Chimera--a visualization system for exploratory research and analysis. *J Comput Chem*, 2004. 25(13): 1605-12.
38. Emsley, P and K Cowtan, Coot: model-building tools for molecular graphics. *Acta Crystallogr D Biol Crystallogr*, 2004. 60(Pt 12 Pt 1): 2126-32.
39. Adams, PD, K Gopal, RW Grosse-Kunstleve, LW Hung, TR Ioerger, AJ McCoy, NW Moriarty, RK Pai, et al., Recent developments in the PHENIX software for automated crystallographic structure determination. *J Synchrotron Radiat*, 2004. 11(Pt 1): 53-5.
40. Croll, TI, ISOLDE: a physically realistic environment for model building into low-resolution electron-density maps. *Acta Crystallogr D Struct Biol*, 2018. 74(Pt 6): 519-530.
41. Pettersen, EF, TD Goddard, CC Huang, EC Meng, GS Couch, TI Croll, JH Morris and TE Ferrin, UCSF ChimeraX: Structure visualization for researchers, educators, and developers. *Protein Sci*, 2021. 30(1): 70-82.

42. Waterhouse, AM, JB Procter, DM Martin, M Clamp and GJ Barton, Jalview Version 2--a multiple sequence alignment editor and analysis workbench. *Bioinformatics*, 2009. 25(9): 1189-91.
43. Garcia-Nafria, J, Y Lee, X Bai, B Carpenter and CG Tate, Cryo-EM structure of the adenosine A(2A) receptor coupled to an engineered heterotrimeric G protein. *Elife*, 2018. 7.